Astron. Astrophys. 358, 332–342 (2000)

ASTRONOMY AND ASTROPHYSICS

An empirical test of different ionization balance calculations in an isothermal solar plasma

R. Allen[1], **E. Landi**[2,3], **M. Landini**[2], **and G.E. Bromage**[1]

[1] Centre for Astrophysics, University of Central Lancashire, Preston, UK
[2] Department of Astronomy and Space Science, University of Florence, Italy
[3] Max-Planck-Institute für Aeronomie, Katlenburg-Lindau, Germany

Received 16 November 1999 / Accepted 24 March 2000

Abstract. By examining solar observations using the Normal Incidence Spectrometer (NIS) within the Coronal Diagnostic Spectrometer (CDS) on board SOHO, an isothermal region in the lower solar corona was chosen for analysis by three different temperature diagnostic techniques. These techniques are the line-ratio method, the Differential Emission Measure and the Emission Measure analysis. All three methods should in theory yield the same temperature. Using these powerful diagnostic methods, the reliability of all widely used ionisation balance calculations, namely those of Shull & Van Steenberg (1982), Arnaud & Rothenflug (1985) (with revisions by Arnaud & Raymond 1992) and Mazzotta et al. (1998) have been empirically tested.

It has been found that the temperature obtained does not depend on the ionization balance calculation used. It is also concluded that the three ionization balance calculations give the same results, within their uncertainties.

A new variant Emission Measure analysis is presented. This provides a diagnostic tool that is stable against any distorting effects arising when a few lines have large deviations from the mean.

Key words: atomic data – Sun: corona – Sun: UV radiation

1. Introduction

The use of EUV emission line diagnostics for astrophysical plasmas has been one of the most widely used techniques to measure the plasma's physical parameters such as electron density and temperature, chemical abundances and plasma Differential Emission Measure. These techniques rely both on spectroscopic observations and on knowledge of a large number of theoretical atomic parameters including transition probabilities, which underpin the line emission processes.

Uncertainties in these theoretical parameters will clearly affect the derived plasma parameters.

Diagnostic tools for investigating the physical parameters of the solar corona have developed markedly during the last few years. Large databases of updated atomic structure and collision data have been created, such as CHIANTI (Dere et al. 1997, Landi et al. 1999) and ADAS (Summers 1993). These are now helping in the analysis of the extensive EUV observations of the solar corona collected by SOHO both with high resolution spectrometers, such as CDS (Harrison et al. 1995) and SUMER (Wilhelm et al. 1995), and with narrow bandwidth imaging telescopes (EIT, Delaboudiniere et al. 1995).

One of the most important parameters in the evaluation of the expected line emission from an optically thin source is the *emitting ion abundance*, since it is responsible for much of the temperature dependence of the line intensity. Temperature, element abundance and Differential Emission Measure diagnostics all largely depend on the assumed ion abundance.

Ion abundances are available in the literature from a few theoretical computations under the assumption of ionization equilibrium. These datasets have been calculated by a number of different authors, yielding sometimes remarkably different results. Differences in the ion fractions may significantly alter the plasma diagnostic results.

In the recent past, Masai (1997) investigated the impact of uncertainties in the ionization and recombination rates on X-ray spectral analyses, finding that differences in the rates led to significant differences in iron abundance and plasma temperature measurements. Phillips & Feldman (1997) have used *Yohkoh* flare observations to check the ion fractions of He-like ions, concluding that the observed spectra were consistent with the adopted ion fractions at the 50% level of precision, and this led to changes to the plasma diagnostic results. Gianetti et al. (2000) have investigated the impact of the use of different ion fractions on the FIP effect and *DEM* studies, finding that ion fraction uncertainties completely alter the diagnostics results.

An assessment of the quality of ion abundance computations is not an easy task, due to the complicated and largely unknown temperature structure of the solar atmosphere as seen along the line of sight. Such an attempt has been made in the past by Cheng et al. (1979a, 1979b), who compare ion abundance calculations from Jordan (1969, 1970), Summers (1974) and Jacobs et al. (1977) by means of Si VIII, Fe XI, Fe XII and Fe XXI line width studies from solar spectra. They find that observations indicate that Summers 1974 ion abundances are probably less accurate than the other two. The same conclusion

Send offprint requests to: r.allen@uclan.ac.uk

has been drawn by Feldman et al. (1981) using EUV line intensities from solar flares. Phillips & Feldman (1997) suggest that Arnaud & Rothenflug (1985) ion abundances for S XV and Ca XIX need to be improved.

Off-limb observations of a quiet solar region should provide a *reasonably isothermal* source with which to investigate abundances of different ionic species. The assumption that the quiet solar corona observed at an appropriate height above the limb is isothermal has been recently verified by Feldman et al. (1999) using SUMER spectra measured at the solar equatorial limb using an east-west slit. Such a simple temperature structure in the emitting plasma facilitates the assessment of the reliability of the ion balance rates.

The aim of this paper is to examine the temperature values measured for an isothermal solar plasma adopting, in turn, three different ionization balance calculations available in the literature:

- Shull & Van Steenberg (1982);
- Arnaud & Rothenflug (1985) incorporating the latest revisions to the iron ions by Arnaud & Raymond (1992);
- Mazzotta et al. (1998)

If no problem arises from atomic physics input a single temperature value must satisfy all the observed lines of different ions of the same element. If the ion balance calculations are incorrect, this will be manifested by a disagreement in the temperature measurements obtained using different ion balance calculations.

A large number of strong lines of ions from the most abundant elements in the solar corona are emitted in the EUV spectral range, and they can be observed by the CDS instrument on SOHO. The wavelength region covered by this instrument allows us to investigate lines formed in a large temperature interval ($10^5 - 3 \times 10^6$ K), making it an ideal instrument for the present study.

This paper is structured as follows. In Sect. 2 the CDS observations are presented and the data reduction is described. Wavelength identifications are reported in Sect. 3. The theory of line emission is outlined in Sect. 4. Sects. 5 to 7 describe the application of three different diagnostic techniques to the observations using in each case the three ionization equilibrium datasets, and the results are discussed in Sect. 8.

2. The observations

The CDS is an imaging spectrograph, whose primary objective is the study of the solar corona through line and continuum emission between 150 Å and 780 Å. It is mounted on the SOHO spacecraft, and can observe the Sun 24-hours a day. Its most important capabilities are therefore simultaneous observation of many lines, monochromatic imaging capability and long duration studies. CDS comprises two distinct spectrometers sharing the same telescope: the Grazing Incidence Spectrometer (GIS) covering four spectral ranges: 151–221, 256–341, 393–492 and 659–785 Å; and the Normal Incidence Spectrometer (NIS) covering the ranges 307–379 and 513–633 Å. Full details of the CDS instrument may be found in Harrison et al. (1995).

In order to maximise the number of spectral lines available, the observational data used for the present analysis covered the full NIS spectrum. A field of view was chosen that included the solar limb and the lower corona in order to be able to select an appropriate isothermal emitting region. The selected position needed to be free from active regions and data faults. The data used were taken on 1997 March 13. The centre of the field of view has heliocentric coordinates (-993, -3.1) arcseconds. The field of view itself has dimensions of 188 x 60 arcseconds and can be seen in Fig. 1.

The data have been reduced, cleaned of cosmic rays and flux calibrated to ergs cm^{-2} s^{-1} str^{-1} using standard routines available in the CDS software. The CDS radiometric calibration adopted in the present work is the revised CDS calibration presented by Lang et al. (1999); this work takes into account both pre-flight measurements (Bromage et al., 1996) and in-flight data from CDS and rocket-borne instruments to determine an absolute intensity calibration for CDS. The Lang et al. (1999) revision results in an adjustment of the NIS 1/NIS 2 relative intensity calibration compared with the Bromage et al. 1996 values. This revision was shown to be necessary by Landi et al. (1997), and is important in the present work, since intensity ratios involving pairs of lines observed in NIS 1 and NIS 2 are used here. The error estimates for the CDS-NIS calibration is between 25–45% for NIS 1 and 25% for NIS 2.

2.1. Choosing an isothermal region

A reasonable isothermal plasma can be selected by looking at a small portion of the corona observed outside the limb in a quiet solar region. The region must be in the corona so that the temperature gradient is small enough.

Observations outside the limb allow the lower, non-isothermal transition region and chromospheric plasma to be excluded from the line of sight.

However line intensity quickly decreases with distance beyond the limb due to the decrease in density, as shown in Fig. 2. Therefore, when looking for an isothermal region, a compromise must be reached between finding a region with as shallow a temperature gradient as possible, on the one hand, and retaining a large number of strong spectral lines for analysis, on the other.

In order to avoid transition region plasma the intensity of the following TR lines was measured as a function of distance from the limb:

- He I 515.6 Å
- He I 522.2 Å
- He I 537.0 Å
- O IV 553.3 Å–555.3 Å
- O V 629.7 Å

The optimum region was selected to be where these were nearly indistinguishable from the background noise, whilst preserving sufficient signal/noise ratio for coronal lines. This was found at a solar X of -989 arcseconds.

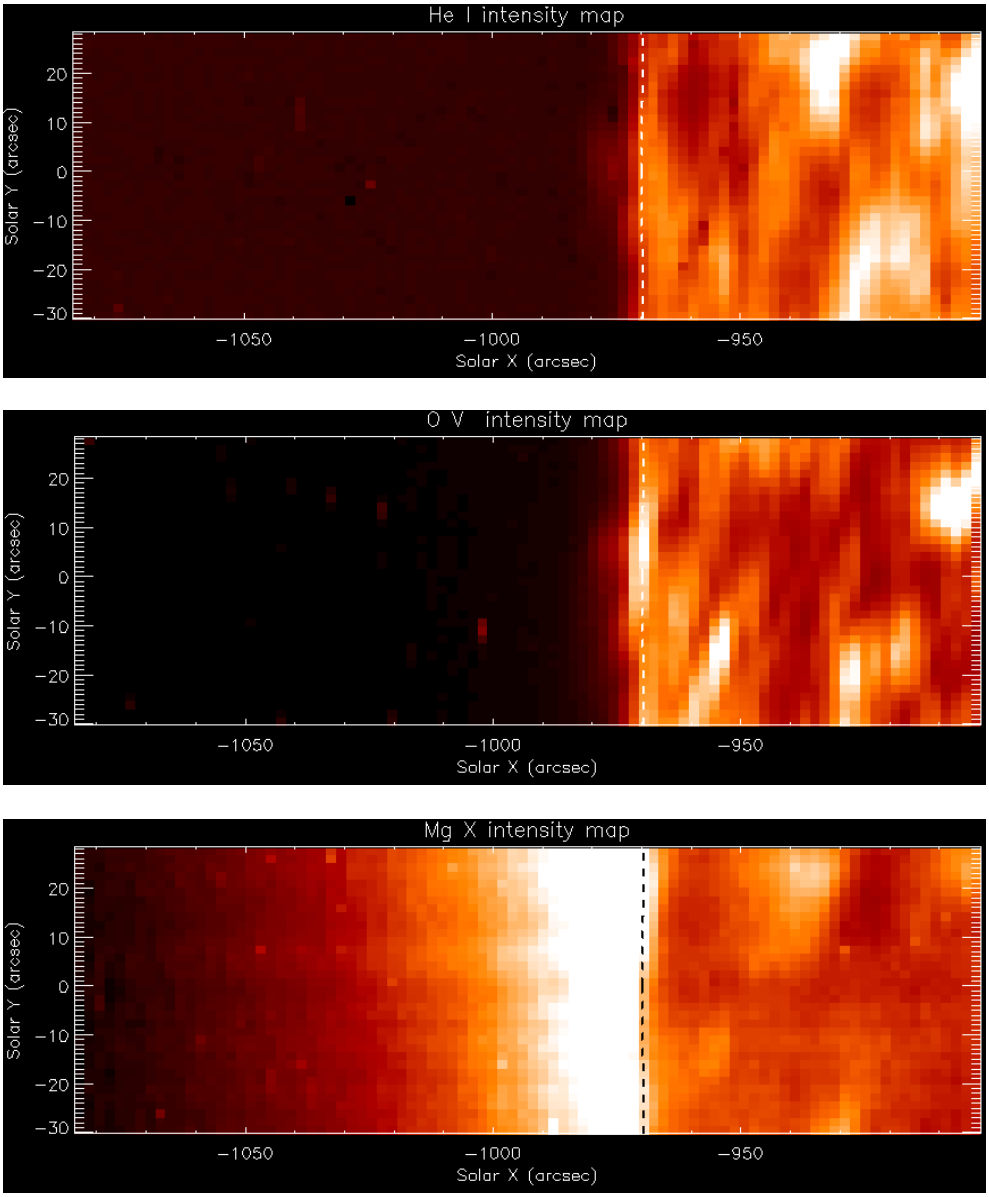

Fig. 1. The field of view of the observational data as seen at temperatures typical of the chromosphere (He I-584.3 Å top panel), the transition region (O V-629.7 Å center panel) and the corona (Mg X-624.9 Å bottom panel). The image spans the 90 slit positions in solarX (188″ in total) from X=0 on the right of the image to X=89 and covers 35 pixels in solarY. The solar limb can clearly be seen as it is much brighter than the disk in coronal light.

In order to average over any inhomogeneities of the observed emission region and to improve the signal/noise ratio further, the two dimensional data arrays were averaged in solar Y. The half length in Y is approximately L = 20000 km on the Sun. Over such a distance, the curved limb differs from a straight line by approximately $dH = \frac{L^2}{2R}$, which is approximately 285 km in the present case, or 1.4×10^{-2} radians. As a consequence, far enough into the corona, each slit position in solar X has a spectrum originating from a single plane-parallel layer of the solar coronal plasma, which may be considered isothermal if the temperature is only a function of radial distance from the solar centre.

3. Wavelength calibration and line identification

The standard CDS wavelength calibration was employed throughout the present analysis. This wavelength calibration is implemented in the CDS/IDL calibration database as "McWhirter - Sept. 1996" and is described by Brooks et al. (1999). As a spectral line reference, a spectral atlas was used, based on previous extensive work on the CDS-NIS carried out by Brooks et al. (1999). Fitted wavelength values and intensities for the lines used here are presented in Tables 1 and 2.

Most of the measured wavelengths show a slight blueshift compared with the laboratory wavelengths adopted by Brooks et al. (1999). The mean observed value is too large to be due to the solar rotation and the individual values do not show any correlation with either wavelength or temperature of line formation. Instead, the effect is most probably due to the dependence of the NIS wavelength zero-point on the CDS optical bench temperature, as suggested by Brooks et al. (1999) (see their Fig. 1) and Gallagher et al. 1999. This effect has been corrected using the method described by Brooks et al. 1999 (Sect. 4).

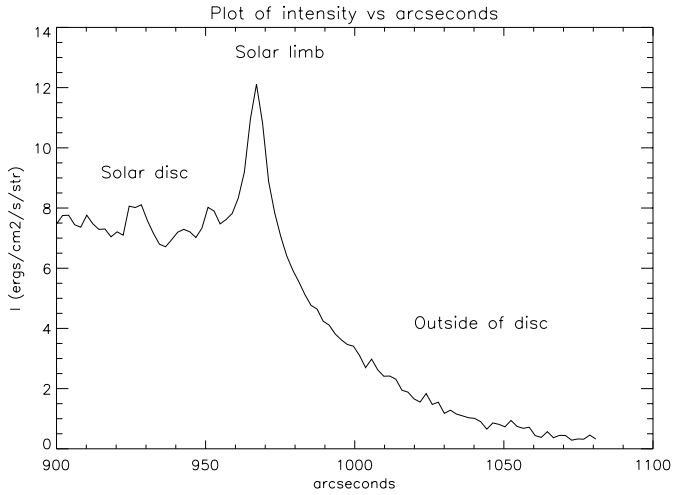

Fig. 2. Fe XIII 348 Å line intensity is plotted vs. distance (arcseconds) from the solar centre.

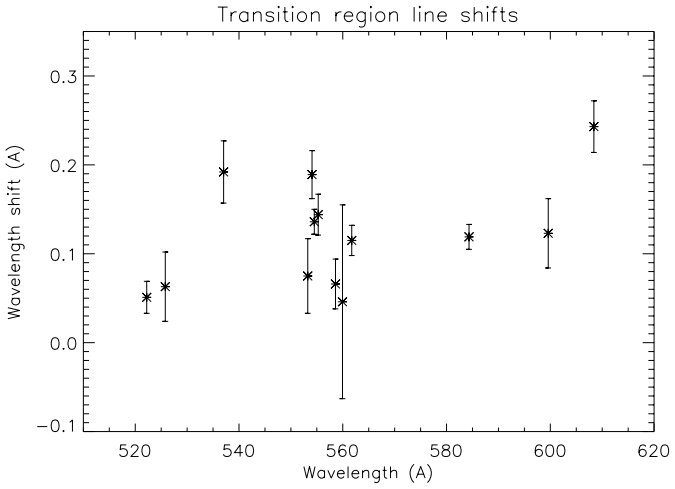

Fig. 3. Wavelength shifts of Transition Region lines observed in the present dataset. The average value of the shift is 0.120 A and its standard deviation is 0.061 A.

3.1. Presence of transition region lines

During the process of line identification, several weak transition region lines were found, none of which should be present in this coronal spectrum. Their presence may be due to scattering either inside the CDS, or by the coronal plasma, or both. This phenomenon may also cause lines such as Mg VII to be artificially enhanced.

The TR lines also show a systematic wavelength shift relative to the true coronal lines. Fig. 3 shows the wavelength shifts of the transition region lines observed in the present dataset. These were calculated *after* the wavelength calibration was corrected for the optical bench effects.

These TR lines were therefore not used for the remainder of the present study.

Table 1. Measured wavelengths and intensities of lines observed in the NIS 1 band.

Ion	Wavelength (Å)	Intensity (erg cm^{-2} s^{-1}str^{-1})
Fe XI	308.490 ± 0.014	8.8 ± 0.7
Mg VIII	311.744 ± 0.005	21.6 ± 1.1
Mg VIII	313.714 ± 0.004	40.0 ± 1.2
Si VIII	314.328 ± 0.004	41.3 ± 1.2
Mg VIII	314.992 ± 0.002	108.6 ± 1.9
Si VIII	316.185 ± 0.003	75.6 ± 1.5
Mg VIII	317.013 ± 0.005	31.2 ± 1.0
Mg VII	318.978 ± 0.047	4.3 ± 0.9
Si VIII	319.808 ± 0.002	122.4 ± 2.0
Fe XIII	320.774 ± 0.041	2.1 ± 0.6
Al VIII	325.317 ± 0.041	2.5 ± 0.6
Al VIII	328.180 ± 0.013	10.7 ± 1.0
Al X	332.744 ± 0.004	32.9 ± 1.4
Mg VIII	335.218 ± 0.005	29.0 ± 1.3
Fe XII	338.274 ± 0.016	7.5 ± 0.8
Mg VIII	338.970 ± 0.005	33.2 ± 1.3
Ca VII	339.874 ± 0.029	3.6 ± 0.7
Fe XI	341.088 ± 0.007	30.9 ± 1.3
Si IX	341.921 ± 0.004	46.4 ± 1.5
Si IX	344.859 ± 0.020	21.5 ± 3.9
Si IX	345.082 ± 0.006	97.5 ± 3.9
Fe X	345.686 ± 0.003	74.8 ± 2.0
Fe XII	346.864 ± 0.016	10.0 ± 1.0
Si X	347.360 ± 0.003	80.4 ± 1.9
Fe XIII	348.087 ± 0.029	4.4 ± 0.8
Fe XI	349.144 ± 0.024	5.5 ± 0.8
Si IX	349.820 ± 0.004	112.4 ± 2.3
Fe XII	352.072 ± 0.005	34.0 ± 1.2
Fe XI	352.634 ± 0.003	74.9 ± 1.8
Al VII	353.720 ± 0.039	2.6 ± 0.7
Si X	355.988 ± 0.003	57.0 ± 1.7
Fe XI	356.500 ± 0.011	11.3 ± 0.7
Al VII	356.903 ± 0.030	3.3 ± 0.5
Fe XI	358.575 ± 0.012	15.2 ± 1.2
Fe XIII	359.677 ± 0.019	4.3 ± 0.6
Mg VII	363.752 ± 0.014	4.5 ± 0.4
Fe XII	364.423 ± 0.003	37.7 ± 1.1
Mg VII	365.159 ± 0.008	15.0 ± 0.7
Fe X	365.512 ± 0.004	36.2 ± 1.1
Mg VII	367.613 ± 0.017	36.5 ± 3.6
Mg IX	368.024 ± 0.002	698.4 ± 15.0
Fe XI	369.129 ± 0.015	22.3 ± 2.2

4. Theory of the intensity integral in an isothermal plasma

The intensity integral of an optically thin emission line is given by

$$I_{ji} = \frac{1}{4\pi}\int_h N_j(X^{+m})A_{ji}h\nu_{ji}dh \quad erg\,cm^{-2}\,s^{-1}\,str^{-1} \quad (1)$$

where $N_j(X^{+m})$ is the number density of ions of element X ionized to degree $+m$ in the j^{th} excited level, and A_{ji} is the Einstein coefficient for the probability of the spontaneous emission of a photon of energy $h\nu_{ji}$. For a transition from j to i,

Table 2. Measured wavelengths and intensities of lines observed in the NIS 2 band. Lines marked with ⋆ are second order lines.

Ion	(Å)	Intensity (erg cm^{-2} s^{-1}str^{-1})
Si X ⋆	516.636 ± 0.026	0.83 ± 0.14
Si XII	520.614 ± 0.009	2.7 ± 0.2
Si X ⋆	543.888 ± 0.024	0.72 ± 0.11
Al XI	550.000 ± 0.005	5.9 ± 0.3
O IV	553.213 ± 0.042	0.55 ± 0.12
O IV	553.846 ± 0.027	1.5 ± 0.2
O IV	554.336 ± 0.014	3.0 ± 0.2
O IV	555.077 ± 0.023	0.92 ± 0.14
Ca X	557.717 ± 0.003	35.7 ± 1.0
Al XI	568.058 ± 0.013	3.5 ± 0.3
Ca X	573.931 ± 0.004	23.8 ± 1.0
Si XI	580.826 ± 0.010	7.0 ± 0.4
Si IX ⋆	581.533 ± 0.037	1.3 ± 0.3
Si IX ⋆	585.616 ± 0.019	2.5 ± 0.3
Si IX ⋆	592.350 ± 0.009	7.3 ± 0.4
Si XI	604.077 ± 0.035	0.74 ± 0.16
Si XI ⋆	606.525 ± 0.006	2.7 ± 0.2
He II ⋆	607.365 ± 0.004	4.6 ± 0.2
Mg X	609.681 ± 0.002	317.7 ± 5.8
Mg VIII ⋆	623.528 ± 0.025	2.0 ± 0.3
Mg X	624.850 ± 0.001	174.8 ± 2.3
Mg VIII ⋆	627.386 ± 0.011	2.8 ± 0.3
O V	629.658 ± 0.006	12.8 ± 0.6

the *Contribution Function* (which contains all the density- and temperature-dependent terms in Eq. 1) may be defined as follows:

$$G(T,N_e)=\frac{N_j(X^{+m})}{N(X^{+m})}\frac{N(X^{+m})}{N(X)}\frac{N(X)}{N_H}\frac{N_H}{N_e}\frac{A_{ji}h\nu_{ji}}{N_e} \qquad (2)$$

(a) (b) (c) (d) (e)

where the terms (a) to (e) are explained below:

(a) Relative population of the excited level (j); this is dependent on atomic physics and is only weakly dependent on temperature, but may be strongly dependent on density.
(b) Relative abundance of the ionic species (i.e. "ion fraction"). This is obtained from the ionization balance calculations. This term is dependent on atomic physics and is very temperature sensitive.
(c) Abundance of the element relative to hydrogen.
(d) Number density of hydrogen relative to the number density of electrons. This is ≈ 0.8 for a completely ionized plasma of standard solar composition.
(e) This term is independent of temperature.

In this work, the CHIANTI database (Dere et al. 1997, Landi et al. 1999) was used to calculate term (a). The three different ion fraction data sets (ionisation equilibrium calculations), namely:

– Shull & Van Steenberg (1982), hereafter SHULL
– Arnaud & Rothenflug (1985), hereafter ARNAUD
– Mazzotta et al. (1998), hereafter MAZZ

were used in turn to calculate term (b); and the element abundances of Feldman (1992) to calculate term(c). Substituting in the Contribution Function into Eq. 1 gives:

$$I_{ji}=\frac{1}{4\pi}\int_h G_{ji}(T,N_e)N_e^2dh \qquad (3)$$

If the emitting region is isothermal ($T = T_c$), and assuming a constant pressure along the line of sight, the Contribution Function can be taken out of the integral:

$$I_{ji}=\frac{G_{ji}(T_c,N_e)}{4\pi}\int_h N_e^2dh \qquad (4)$$

The remaining integral is known as the Emission Measure ($\langle EM\rangle$), which, in an isothermal case, is independent of temperature:

$$I_{ji}=\frac{G_{ji}(T_c,N_e)}{4\pi}\langle EM\rangle \qquad (5)$$

Generally, however, the observed emission originates from a plasma which is not strictly isothermal. As we have assumed that there is no plasma structure in the present data set and the temperature dependence of h is continuous, a change of variables to dT is possible. Thus, applying Eq. 3 to density-insensitive lines, and changing the variables to dT results in:

$$I_{ji}=\frac{1}{4\pi}\int_T G_{ji}(T)\,N_e^2\frac{dh}{dT}\,dT \qquad (6)$$

Under these conditions, the term $N_e^2\frac{dh}{dT}$ is known as the Differential Emission Measure (*DEM*) and is written as $\psi(T)$:

$$I_{ji}=\frac{1}{4\pi}\int_T G_{ji}(T)\psi_{ji}(T)dT \qquad (7)$$

In the special case of a strictly isothermal plasma, dT is equal to 0 and the above procedure fails. However due to the finite dT interval used in the DEM evaluation and the finite width of the G(T) functions, an isothermal solution appears as a very narrow function, almost a Dirac delta function, when *DEM* is plotted versus temperature.

A *DEM* analysis was performed on the present data in order to verify that the emitting plasma was really isothermal; the results are described below.

5. The differential emission measure (*DEM*)

To verify that the chosen emitting region was isothermal, the *DEM* of the plasma was measured using all the density insensitive lines observed in the present dataset, following the iterative technique described by Landi & Landini (1997), to which the reader is referred for further details.

This analysis was repeated using the three different ion fraction datasets SHULL, ARNAUD and MAZZ, in order to assess the impact of differences in these three datasets on the *DEM* shape, and on the value of the temperature where the *DEM* peaks. In all cases element abundances were taken from Feldman (1992).

The Mg VII lines were not used in the analysis, since these showed values of $I_{obs}/I_{theoretical}$ which were too high. This behaviour is independent of the ion fractions dataset. The presence of significant instrument-scattered light, as mentioned in Sect. 3.1, might be the cause of this.

The resulting *DEM* curves are displayed in Fig. 4, for the three different ionization balance calculations.

The *DEM* analysis can be used to determine possible variations of the abundance of some elements relative to the others, as shown by Landi & Landini (1997,1998). Moreover, the use of three different ion balance datasets allows us to investigate the dependence of the measured abundance corrections on the choice of the ion fraction dataset. A more complete study on this topic can be found in Gianetti et al. (2000).

Only the Ca X lines required, in all three cases, a revision of the Ca abundance relative to the other elements; however, the amount of the correction changes from $\simeq$ 8–10 (SHULL and ARNAUD) to around 2 (MAZZ). Such discrepancies were noted in the past by Landi & Landini (1998) and Del Zanna & Bromage (1999), who suggest that calcium abundance is responsible for this. However, Smith et al. (1985) pointed out that the dielectronic recombination rates used in the SHULL and ARNAUD are incorrect for the Ne-like ions, and that this altered the corresponding Na-like ion abundances. This might explain why results obtained with the MAZZ dataset, who adopt different rates for Ne-like dielectronic recombination, show that Ca X requires smaller changes to its relative abundance.

No other corrections to the relative abundance of other elements were found.

Aluminum ions show some problems, which cannot be ascribed to Al chemical abundance. In fact, the theoretical intensities for Al VII and Al VIII are systematically larger than their observed values, while those of the Al X and Al XI ions are in agreement. The amount of the disagreement depends largely on the ion fraction dataset, but the trend in the same in all cases. The reason for this behaviour is not clear.

Fe XIII lines always show too low $I_{obs}/I_{theoretical}$ relative to the lines formed at similar temperature, and this behaviour does not change with the ion fraction datasets. A similar, but much less pronounced trend is also shown by Fe XII relative to Al X and Si X. Fe X,XI lines on the contrary show a reasonable agreement with Mg, Si and Al X lines, so that abundance problems are not the cause. It is to be noted that Feldman et al. (1999) have reported that Fe line intensities decrease at the solar limb faster than those of the lighter ions, due to gravitational settling. However, the emitting region selected in the present dataset is too close to the solar disc to have significant Fe depletion due to this effect. Also, this would not explain the agreement found with Fe X,XI. Young et al. (1998) and Landi & Landini (1997) report some problems with Fe XIII line ratios which could be ascribed to atomic physics problems, which could partly explain the problems encountered in the present work. However, it is also possible that ion fraction problems for Fe XIII play a role.

It is interesting to note that a *DEM* analysis carried out for only Fe lines yields a *DEM* curve whose peak temperature is

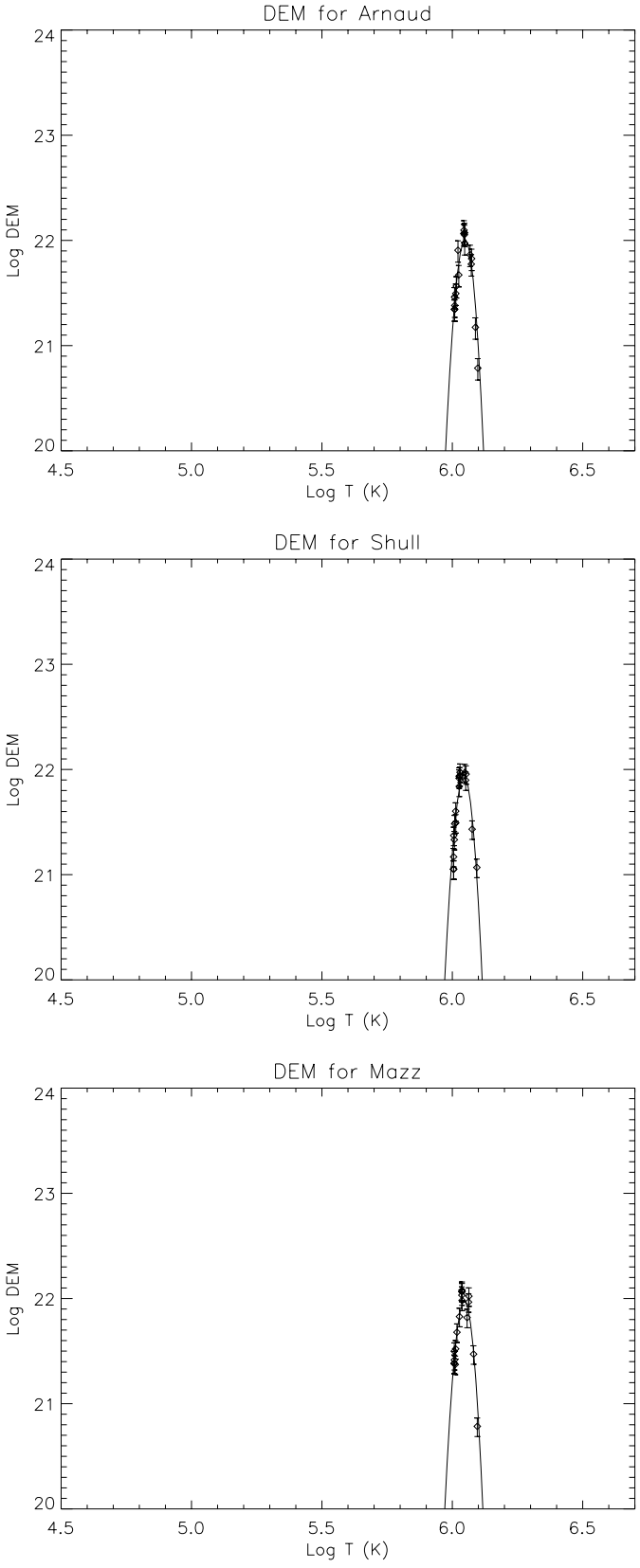

Fig. 4. *DEM* curves for the emitting region determined using the three different ionization balance calculations. The temperature of each line in the plot is given by the average of the temperature weighted by the *DEM* and emissivity curves.

very similar to the one obtained using all the lines, and the differences between the two curves are only in their high temperature tails and in the peak value of the *DEM*, which is slightly lower for the *DEM* obtained with Fe lines only.

Feldman et al. (1998) report that all Li-like ions show a systematic excess in theoretical emissivities relative to all the other ions of the other isoelectronic sequences. Similar results have also been found by Del Zanna (1999) and Judge et al. (1995). However, no trace of this problem is found in the present work, where the intensities of Mg X, Al XI and Si XII have been used, for any of the ion fraction datasets adopted.

The *DEM* analysis shows that changing the ion fraction datasets may cause large differences in the behaviour of single ions, but the overall shape of the nearly-isothermal *DEM* curve is not changed significantly. The *DEM* plots show that the plasma is isothermal within 0.1 in log T and that the chosen emitting region is therefore appropriate for further analysis.

The temperature values obtained using the three *DEM* analyses are very similar, and are reported in Table 5 (top). Their similarity indicates that the use of *DEM* analysis for temperature diagnostics in a nearly isothermal plasma is robust against changes in the ion fraction datasets.

The electron temperature measured by the *DEM* analysis is only slightly lower than reported by Feldman et al. (1999) from SUMER observation of quiet off-limb plasma.

6. Line ratio diagnostics applied to isothermal plasmas

6.1. The line ratio diagnostic of temperature

In the special case of an isothermal plasma the intensity of an optically thin line is given by Eq. 5 alone, so that the ratio of two intensities I_1/I_2 reduces to:

$$\frac{I_1}{I_2} = \frac{G_1(T_c, N_e)\,\langle EM\rangle}{G_2(T_c, N_e)\,\langle EM\rangle} = \frac{G_1(T_c, N_e)}{G_2(T_c, N_e)} \tag{8}$$

where $T = T_c$ is the temperature of the emitting isothermal plasma. In general this result is dependent on both temperature and density. It follows that in order to obtain a reliable temperature value from the line ratio method, it is necessary to use density-*insensitive* line ratios. In some cases it is possible to avoid the density dependence by summing two density dependent lines and calculating the ratio with a density insensitive line, because the summed spectral feature depends on the electron density very weakly. However, the residual density dependence makes these ratios less reliable for temperature diagnostics, and they are not necessary in the present study where many other suitable line pairs are found.

It is necessary to choose lines of the same element in order to avoid problems arising from element abundances. Due to the strong temperature dependence of the relative abundance of the ionic species, it is best to use lines from different stages of ionization. This strong dependence causes the uncertainties in the measured temperature values to be very low even when very weak lines are used. Moreover, most of the theoretical ratios change by a factor 2–3 in Log T intervals of 0.1, so that the $\simeq$30% uncertainty usually quoted in the literature for ionization and recombination rates does not increase the uncertainties of the measured temperatures.

The CHIANTI database provided suitable line pairs for temperature diagnostics, selected from the observed lines (Table 1 and 2). The following lines are density insensitive over the relevant temperature range and are thus suitable for the line ratios:

Al	X	-	332.789 Å
	XI	-	550.029 Å
Fe	X	-	345.722 Å
	X	-	365.541 Å
	XI	-	341.112 Å
	XI	-	356.518 Å
	XI	-	358.620 Å
Mg	VIII	-	335.252 Å
	VIII	-	339.005 Å
	IX	-	368.070 Å
	X	-	609.792 Å
	X	-	624.940 Å

In order to verify the density insensitivity of various line pairs, the ratios were calculated for three sample values of the density typical of quiet and active solar regions (10^8, 10^9 and 10^{10} cm^{-3}). The temperature values obtained are tabulated in Table 3 for the three different ionization balance calculations.

Any density sensitivity present for these lines affects the log temperature values by less than 0.01.

The mean Log T values calculated for each of the ionization balance calculations are reported in Table 5 (bottom).

6.2. The line ratio diagnostic of density

It is unnecessary to perform a density diagnostic on the data for the purpose of distinguishing between different ionization balance calculations, because the ones we use do not include density effects. A density diagnostic does, however, act as another check of the isothermal nature of the chosen emitting region, since any isothermal region of the corona where no plasma structures are observed should also be fairly homogenous in electron density, assuming hydrostatic equilibrium. The theory behind taking line ratios as a density diagnostic in an isothermal plasma can be explained from Eq. 8, where, of course, *temperature insensitive* ratios must be used. However, *weakly* density sensitive ratios must be avoided as they can give very uncertain results. To obtain temperature insensitive ratios line pairs of the same ion must be used. From the list of possible density sensitive lines, 12 lines ratios are appropriate for the density range of interest ($10^8 - 10^{10}$ cm^{-3}). These are listed in Table 4. Line ratios involving Mg VII lines have been discarded because they are probably contaminated by instrument scattered light.

There is however one further complication that needs to be mentioned before taking ratios. The contribution functions given by the CHIANTI database have been calculated on the assumption that the absorption of photospheric photons by transitions between levels of the ground configuration has a negligible effect on level population calculations. This is an adequate assumption for most purposes in the quiet Sun, since electron

Table 3. The table shows the calculated Log T values from the line ratio method for the three different ionization balance calculations. The mean temperature values are shown in the last row.

	ARNAUD			SHULL			MAZZ		
LINE RATIO	Log(T) at Log(Ne) =8	Log(T) at Log(Ne) =9	Log(T) at Log(Ne) =10	Log(T) at Log(Ne) =8	Log(T) at Log(Ne) =9	Log(T) at Log(Ne) =10	Log(T) at Log(Ne) =8	Log(T) at Log(Ne) =9	Log(T) at Log(Ne) =10
$\frac{Al\ X\ (332)}{Al\ XI\ (550)}$	6.05	6.05	6.04	6.05	6.05	6.04	6.08	6.07	6.07
$\frac{Fe\ X\ (345)}{Fe\ XI\ (341)}$	5.99	6.00	6.00	6.05	6.05	6.05	6.00	6.01	6.00
$\frac{Fe\ X\ (345)}{Fe\ XI\ (356)}$	5.96	5.97	5.96	6.01	6.02	6.01	5.97	5.97	5.97
$\frac{Fe\ X\ (345)}{Fe\ XI\ (358)}$	5.97	5.97	5.97	6.02	6.02	6.02	5.97	5.98	5.97
$\frac{Fe\ X\ (365)}{Fe\ XI\ (341)}$	5.98	5.98	5.98	6.03	6.04	6.03	5.99	5.99	5.99
$\frac{Fe\ X\ (365)}{Fe\ XI\ (356)}$	5.95	5.96	5.91	6.00	6.00	6.00	5.95	5.96	5.95
$\frac{Fe\ X\ (365)}{Fe\ XI\ (358)}$	5.95	5.96	5.91	6.00	6.01	6.00	5.96	5.96	5.96
$\frac{Mg\ X\ (609)}{Mg\ VIII\ (335)}$	6.02	6.02	6.02	6.02	6.02	6.02	6.02	6.02	6.02
$\frac{Mg\ X\ (609)}{Mg\ VIII\ (339)}$	6.03	6.03	6.03	6.03	6.03	6.03	6.03	6.03	6.03
$\frac{Mg\ X\ (624)}{Mg\ VIII\ (335)}$	6.03	6.03	6.03	6.03	6.02	6.02	6.02	6.02	6.02
$\frac{Mg\ X\ (624)}{Mg\ VIII\ (339)}$	6.03	6.03	6.03	6.03	6.03	6.03	6.03	6.03	6.03
$\frac{Mg\ IX\ (368)}{Mg\ X\ (609)}$	6.01	6.01	6.01	6.02	6.01	6.01	6.05	6.05	6.05
$\frac{Mg\ IX\ (368)}{Mg\ X\ (624)}$	6.02	6.02	6.02	6.03	6.02	6.02	6.06	6.06	6.06
$\frac{Mg\ IX\ (368)}{Mg\ VIII\ (335)}$	6.03	6.04	6.04	6.02	6.03	6.03	5.98	5.99	5.99
$\frac{Mg\ IX\ (368)}{Mg\ VIII\ (339)}$	6.05	6.05	6.05	6.04	6.04	6.04	6.00	6.00	6.00
$\langle LogT \rangle$ =	6.01	6.01	6.00	6.03	6.03	6.02	6.01	6.01	6.01

excitation is a much more efficient populating process at coronal densities for most ions. However some of the present observed ions have critical densities which are comparable with the density range of interest.

By critical density is meant the maximum electron density at which absorption by photons in the photon field is important in the statistical equilibrium calculations of the level populations for the ground configuration. The absorption of photons must therefore be incorporated into the calculations, and that has been done in the present study.

The density values determined from the selected line pairs are given in Table 4.

7. An emission measure analysis for isothermal plasmas

From Eq. 5, for an isothermal plasma the Emission Measure can be evaluated as:

$$\langle EM \rangle = 4\pi \, \frac{I}{G(T, N_e)} \tag{9}$$

Therefore the graph $\frac{I}{G}$ vs. T for any given spectral line supplies the $\frac{1}{4\pi} \langle EM \rangle$ value which, for each temperature, satisfies the measured intensity.

At this point, we still do not know what the plasma $\langle EM \rangle$ value is, but by over-plotting I/G of another spectral line, the two curves should both pass through the point at $\left(T_c, \frac{1}{4\pi} \langle EM \rangle (T_c)\right)$, i.e., the two curves should cross at that point. This overplotting can be repeated as many times as there are spectral lines from the emitting region.

Table 4. The electron densities obtained from the line ratio diagnostic for density, including the mean value and a standard deviation of the mean.

LINE RATIO	ELECTRON DENSITY AT $Log_{10}(T) = 6.01$	ELECTRON DENSITY AT $Log_{10}(T) = 6.02$
Fe XI $\frac{341.09}{349.14}$	8.38	8.40
Fe XI $\frac{349.14}{352.63}$	8.98	8.98
Fe XI $\frac{349.14}{356.50}$	8.80	8.80
Fe XI $\frac{349.14}{358.57}$	8.74	8.74
Fe XI $\frac{349.14}{369.13}$	8.98	9.00
Fe XIII $\frac{348.09}{320.77}$	8.64	8.66
Fe XIII $\frac{348.09}{359.68}$	8.80	8.80
Si IX $\frac{344.86}{349.82}$	8.78	8.78
Si IX $\frac{345.08}{349.82}$	8.34	8.34
Si IX $\frac{341.92}{349.82}$	8.52	8.54
Si X $\frac{347.36}{355.99}$	8.54	8.56
MEAN DENSITY =	8.7±0.2	

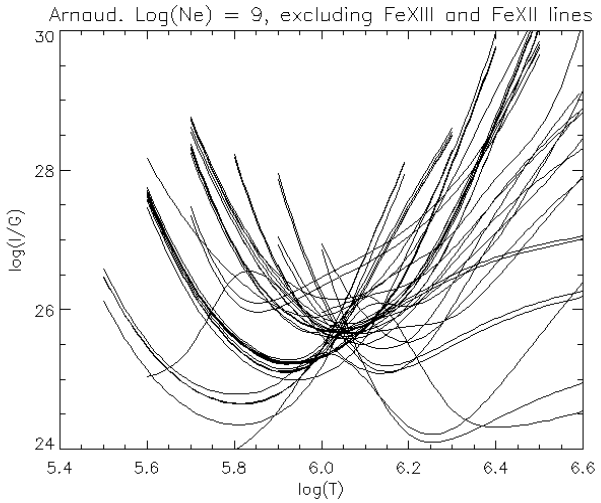

Fig. 5. The I/G functions of all the available spectral lines (but without Fe XII and Fe XIII observed in the chosen plasma plotted against varying temperature.

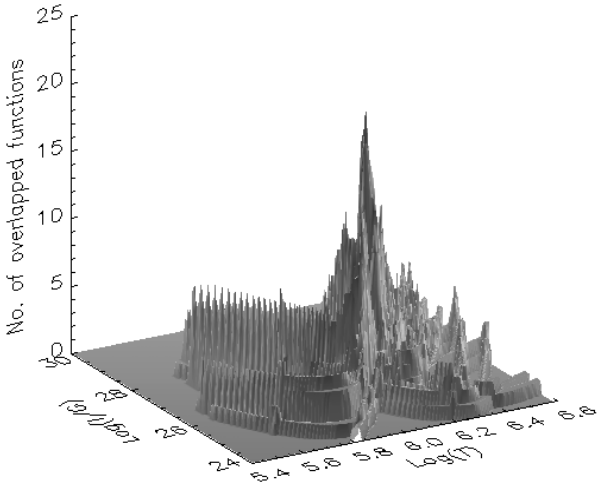

Fig. 6. The Emission Measure Analysis is shown here for the Arnaud & Rothenflug (1985) / Arnaud & Raymond (1992) ionization balance calculations. One peak clearly dominates the graphic - this being the point of the maximum number of overlapping areas.

Table 5. The temperatures calculated using the *DEM* (*top*) and the Line Ratio (*bottom*) methods. The uncertainties in the Log T values from the *DEM* curve are simply taken as from the temperatures at the extremes from each *DEM* plot in Fig. 4.

Differential Emission Measure		
	$Log(T)$	$\sigma Log(T)$
Arnaud	6.03	$\pm$0.05
Shull	6.05	$\pm$0.05
Mazz	6.01	$\pm$0.05
Line Ratio Method		
	$Log(T)$	$\sigma Log(T)$
Arnaud	6.01	$\pm$0.04
Shull	6.03	$\pm$0.02
Mazz	6.01	$\pm$0.04

In an isothermal case, if there are no problems arising from atomic physics or ionization balance calculations, the $\frac{I}{G}$ functions should all cross at the same temperature.

An example is displayed in Fig. 5 using all the coronal lines listed in Tables 1 and 2; only the lines emitted by Fe XII and Fe XIII were not included (see Sect. 5). The ionization balance calculations used for Fig. 5 are those of Arnaud & Rothenflug (1985) / Arnaud & Raymond (1992) for an electron density of 10^9 cm^{-3}. Note that most lines cross inside a small region in (I/G,T) space but there are also a few crossing points relatively far outside this region: these discrepancies are most likely due to the problems outlined in Sect. 5.

7.1. The emission measure analysis as a temperature diagnostic

The mean temperature can be obtained by considering the crossing points of each pair of lines in turn and then calculating the mean of all the crossing temperatures. The values resulting from this Emission Measure analysis carried out using the three different ion fraction datasets are reported in Table 6 (top).

A more meaningful approach is to consider for each line the "stripe" in (I/G,T) space obtained by plotting the observed intensity plus and minus the uncertainty. Each pair of observed lines thus defines an area in the Log $\frac{I}{G}$ vs. $logT$ plot, and the region common to the largest number of stripes supplies the best temperature and emission measure, together with their uncertainties.

One example of this technique is displayed in Figs. 6 and 7, where the Contribution Functions have been calculated using the ARNAUD dataset for ion fractions. A clear structure can be distinguished and a single dominant temperature peak is clearly visible.

This example shows one most prominent region, the other regions being far less prominent. In the case of the SHULL data, there are two prominent regions in the plot for a density of $Log(N_e)$ = 8 but only one for $Log(N_e)$ = 9. This is illustrated in Fig. 8 for $Log(N_e)$ = 8.

Since each line generates a "stripe" in the I/G vs T space, its width is given by the uncertainty associated with the line. As a consequence, the new $\langle EM \rangle$ analysis indicates regions in $\langle EM \rangle$ - T space that are delineated by these uncertainties. Therefore, a way of determining the uncertainties on the obtained $(T_e, \langle EM \rangle)$ values would be to find the size of the temperature interval at which, for example, 68% (or 1/e) of the lines cross. The resulting temperature and $\langle EM \rangle$ values are given in Table 6 (bottom).

8. Discussion

Tables 5 and 6 summarise the results obtained from the three different temperature diagnostic methods used.

These tabulated results clearly show we have an isothermal plasma in the region of analysis. Furthermore, they show that

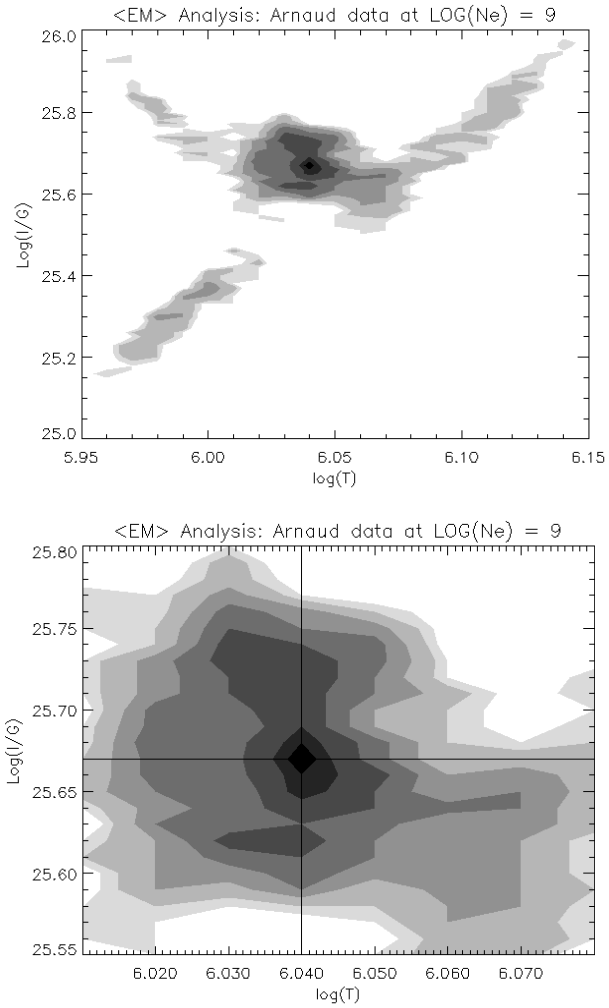

Fig. 7. The new variant of Emission Measure Analysis is shown here for the Arnaud & Rothenflug (1985) / Arnaud & Raymond (1992) ionization balance calculations. The darkest shades correspond to 21 or more overlapping areas, the next darkest corresponds to 20 or more, the next corresponds to 18 or more, the next ones to 16,14,12,11 and 10 or more overlapping areas respectively.

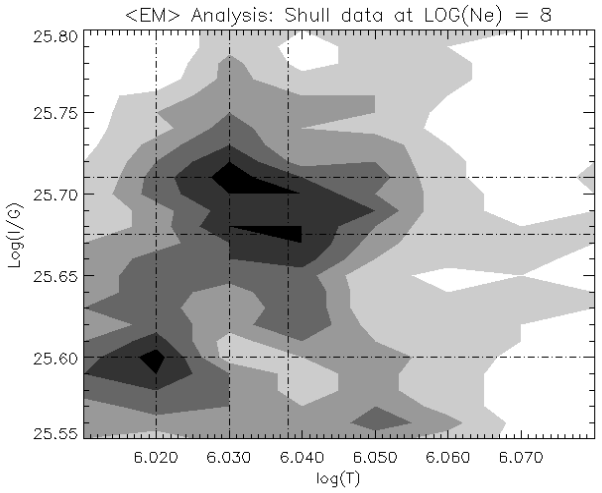

Fig. 8. The new variant of Emission Measure Analysis is shown here for the Shull & Van Steenberg (1982) ionization balance calculations. The darkest shades correspond to 18 or more overlapping areas, the next darkest corresponds to 16 or more, the next corresponds to 14 or more, the next ones to 16,14,12,9 and 7 or more overlapping areas respectively.

Table 6. *Top*: The mean values for the temperature and the $\langle EM \rangle$ for an electron density of $Log(N_e) = 9$ obtained calculating the mean of the temperature of $\frac{I}{G}$ crossing points for each pair of lines. The quoted uncertainties are the standard deviations from the mean values. *Bottom*: The temperatures and values obtained from the "stripe" analysis. Uncertainties are given by the width of the area where 68% of the stripes cross.

EM Analysis - mean of the crossing points				
	$Log(T)$	$\sigma Log(T)$	$Log(\langle EM \rangle)$	$\sigma Log(\langle EM \rangle)$
Arnaud	6.04	$\pm$0.12	27.05	$\pm$0.64
Shull	6.04	$\pm$0.11	26.95	$\pm$0.58
Mazz	6.04	$\pm$0.15	27.14	$\pm$1.01
"Stripe" Emission Measure Analysis				
	$Log(T)$	$\sigma Log(T)$	$Log(\langle EM \rangle)$	$\sigma Log(\langle EM \rangle)$
Arnaud	6.04	$\pm$ 0.03	26.78	$\pm$ 0.10
Shull	6.03	$\pm$ 0.02	26.76	$\pm$ 0.10
Mazz	6.02	$\pm$ 0.03	26.71	$\pm$ 0.15

for any given ionization balance calculation, the temperature diagnostic techniques used all agree with one another within the uncertainty values that are present. This confirms that the diagnostic methods used are consistent within their uncertainty values for an isothermal plasma.

The results show also that for any given diagnostic technique, all three ionization balance calculations gave the same temperature value and uncertainty.

The $\langle EM \rangle$ analysis indicates that the scatter about the mean values for MAZZ is large compared to those of SHULL and ARNAUD, which are relatively similar in size, although the SHULL data had slightly less, for both electron density values of N_e = 8 and N_e = 9. The "stripe" $\langle EM \rangle$ analysis shows prominent peaks in the data and regions of concentration in I/G - T space, that agreed with the temperature values of the line ratio method and the *DEM*. This is a very strong confirmation that the coronal region being analysed is isothermal, and that the use of different ionization datasets does not introduce any further uncertainty on the results obtained.

9. Conclusions

The analysis in the present work has given the following results:

1. The emitting plasma can be considered as isothermal; the electron temperature measured in the present work is 1–1.1 $\times$ 10^6 K. This value is only slightly lower than reported by Feldman et al. (1999) using SUMER data;
2. For any given ion balance calculation, the three different diagnostic techniques used in the present work (namely, the *DEM* analysis, emission line intensity ratio and a variant Emission Measure analysis) provide the same electron

temperature. This is a confirmation that these diagnostic techniques lead to consistent results, and are robust against changes in the ion fractions, at least in the case of an isothermal plasma;

3. For any given diagnostic technique, changes in the ion fraction datasets do not alter the final temperature measurements, so that uncertainties in the ion fractions should not be considered a major source of uncertainty in temperature diagnostics of an isothermal plasma;
4. Changes in ion fractions may cause large differencies in the results for single ions. The most striking example is given by Ca X, where MAZZ ion fractions indicate that element abundance for calcium needs a much smaller correction than indicated by using ARNAUD and SHULL datasets;
5. Fe XIII and, to a lesser extent, Fe XII show systematic problems relative to the ions of other elements formed at similar temperatures. As this behaviour is common to all three different ion fraction datasets, it is possible that uncertainties in the excitation and de-excitation coefficients may play a role;
6. A new variant Emission Measure analysis has been presented, which is stable against any distorting effects arising when a few lines have large deviations from the mean.

Acknowledgements. We would like to thank the referee, Dr. J.Raymond, for his very helpful comments on the maniscript. R.Allen would like to thank the University of Florence and the Astrophysical Observatory of Arcetri for hospitality and invaluable support, and the EU Socrates student exchange programme for financial support. The support of the Italian Space Agency (ASI contract RS-96.141) is acknowledged by E.Landi. SOHO is an ESA/NASA project.

References

Arnaud M., Raymond J.C., 1992, ApJ 398, 394
Arnaud M., Rothenflug R., 1985, A&AS 60, 425
Brooks D.H., Fischbacher G.A., Fludra A., et al., 1999, A&A 347, 277
Bromage B.J.I., Breeveld A.A., Kent B.J., Pike C.D., Harrison R.A., 1996, UCLan Report CFA/96/09
Cheng C.-C., Doschek G.A., Feldman U., 1979a, ApJ 227, 1037
Cheng C.-C., Feldman U., Doschek G.A., 1979b, ApJ 233, 736
Delaboudiniere J.P., Artzner G.E., Brunaud J., et al. 1995, Sol. Phys. 162, 291
Del Zanna G., Bromage B.J.I., 1999, J. Geoph. Res. 104, 9753
Del Zanna G., 1999, Ph.D. Thesis, Univ. of Central Lancashire
Dere K.P., Landi E., Mason H.E., Monsignori Fossi B.C., Young P.R., 1997, A&AS 125, 149
Feldman U., Doschek G.A., Cowan R.D., 1981, MNRAS 196, 517
Feldman U., 1992, Physica Scripta 46, 202
Feldman U., Schühle U., Widing K.G., Laming M.J., 1998, ApJ 505, 999
Feldman U., Doscheck G.A., Schühle U., Wilhelm K., 1999, ApJ 518, 500
Gallagher P.T., Phillips K.J.H., Harra-Murnion L.K., Baudin F., Keenan F.P., 1999, A&A 348, 251
Gianetti D., Landi E., Landini M., 2000, A&A, submitted
Harrison R.A., Sawyer E.C., Carter M.K., et al. , 1995, Sol. Phys. 162, 233
Jacobs V.L., Davis J., Kepple P.C., Blaha M., 1977, ApJ 211, 605
Jordan C., 1969, MNRAS 142, 501
Jordan C., 1970, MNRAS 148, 17
Judge P.G., Woods T.N., Brekke P., Rottman G.J., 1995, ApJ 455, L85
Landi E., Landini M., 1997, A&A 327, 1230
Landi E., Landini M., 1998, A&A 340, 265
Landi E., Landini M., Pike C.D., Mason H.E., 1997, Sol. Phys. 175, 553
Landi E., Landini M., Dere K.P., Young P.R., 1999, A&AS 135, 339
Lang J., Kent B.J., Breeveld A.A., et al., 1999, RAL Technical Report, RAL-TR-1999-036
Masai K., 1997, A&A 324, 410
Mazzotta P., Mazzitelli G., Colafrancesco S., Vittorio N., 1998, A&AS 133, 403
Phillips K.J.H., Feldman U., 1997, ApJ 477, 502
Shull J.M., Van Steenberg M., 1982, ApJS 48, 95 and ApJS 49, 351
Smith B.W., Raymond J.C., Mann J.B., Cowan R.D., 1985, ApJ 298, 898
Summers H.P., 1974, MNRAS 169, 663
Summers H.P., 1993, JET Joint Undertaking Report JET-IR(93)06
Young P.R., Landi E., Thomas R.J., 1998, A&A 329, 291
Wilhelm K., et al. , 1995, Sol. Phys. 162, 189